Supporting Information

Bifunctional Galvanics Hinder Bacterial Adhesion while Boosting the Functions of Bone Cells **

Huiliang Cao*, Kaiwei Tang, Xuanyong Liu*

Dr. Huiliang Cao, Mr. Kaiwei Tang, Dr. Xuanyong Liu
State Key Laboratory of High Performance Ceramics and Superfine Microstructure,
Shanghai Institute of Ceramics, Chinese Academy of Sciences,
No.1295 Dingxi Road, Shanghai, 200050, China
E-mail: xyliu@mail.sic.ac.cn (X. L.); hlc@mail.sic.ac.cn (H. C.)
ORCID
Huiliang Cao: 0000-0002-5209-4497
Kaiwei Tang: 0000-0003-4938-0967
Xuanyong Liu: 0000-0001-9440-8143

[**] This work was jointly supported by grants from the National Natural Science Foundation of China (31370962 and 31670980), the Shanghai Rising-Star Program (15QA1404100), the Shanghai Committee of Science and Technology (17441904000), and the Youth Innovation Promotion Association CAS (2015204).

Content

1 Experimental

1.1 Material preparation and Characterizations

Dual-PIII Treatment: Commercial pure titanium substrates (10 mm or 20mm square plates with a thickness of 1mm) were polished mirror finish. And the silver and/or calcium were/was introduced on the substrates by using the filtered cathodic arc sourced plasma immersion ion implantation (PIII) technique. The procedure for single cathodic arc sourced PIII and the interactions between single plasma and the substrate were detailed in our previous reports.[1, 2] In order to simultaneously introduce silver and calcium, the plasma immersion ion implantation equipment was set up with two cathodic-arc sources (Dual-PIII process), which synchronously produces positively charged atoms of the corresponding metals, and accelerates the energetic atoms bombarding into the negatively biased titanium substrates (**Scheme S1**). After PIII, the samples were immediately vacuum-sealed in plastic bags for storage.

Characterizations of the Surface Features: Scanning electron microscopy (SEM, JSM-6700F) was carried out to reveal the surface morphology of the samples. The cross-sectional transmission electron microscopy of the samples was performed on FEI Tecnai G2 F20. The TEM samples were prepared by focused ion beam (FIB, FEI Helios). The chemical states and depth profiles of silver and calcium were determined by X-ray photoelectron spectroscopy (XPS, PHI 5802).

Proton Consumption Potential: The proton consumption potential of the samples were evaluated by using the electrochemical technique, in which the electrocatalytic activity of the samples towards the hydrogen evolution reaction (HER) was evaluated

in the phosphate buffer solution (PBS) by using the linear potential sweep voltammetry (LSV, CHI760C, a saturated calomel electrode as the reference electrode and a graphite rod as the counter electrode), i.e., by scanning the potential towards the negative direction, starting from the corrosion potential down to a potential of -2 V at a scan rate of 0.002 V/s. Before LSV, the open circuit potential as a function of time was carried out for 400 seconds to reach a quasi-stationary state.

Calcium Production Potential: The production potential of calcium (together with silver) from the samples were monitored by incubating them statically in 5 ml physiological saline (0.9% NaCl) at 37 ^{o}C for various periods of durations, and the amount of silver or calcium in the resulted liquids were determined by inductively-coupled plasma optical emission spectrometry (ICP-OES, Vista AX).

1.2 Assays for evaluating the responses of bacterial cells

Cell Morphology Evaluation: 0.06 ml of bacterial solution, at a concentration of 10^8 cfu/ml (Escherichia coli, E. coli, ATCC 25922), was put on each of the 10 mm square samples, and incubated at 37 °C for 24 h, fixed with 3% glutaraldehyde solution (pH=7.4, Gibco, Invitrogen) overnight, and then dehydrated in a series of ethanol solutions (30, 50, 75, 90, 95, and 100 v/v%) for 10 min each sequentially, with the final dehydration conducted in absolute ethanol (twice) followed by drying in the hexamethyldisilizane (HMDS) ethanol solution series. The samples, after being golden coated, were observed on SEM.

Reduction Rate Calculation: The bacterial seeding procedure was the same as that described in *Cell Morphology Evaluation*. The samples, after being incubated at 37 °C for 24 h, were gently rinsed with physiological saline, put into test tubes with 5 ml

physiological saline each, and vigorously vortexed for over 60 s to detach the bacterial cells. Then, the corresponding solution was diluted serially in ten-fold steps with sterile saline, and 200 μl of each diluted bacterial suspensions was cultured on Luria–Bertani (LB) agar plates, and the bacterial colonies were counted after being incubated at 37 ^{o}C overnight. Finally, the reduction rate (R) was calculated according to: $R = (C_{Ti} - C_i)/C_{Ti}$, C_{Ti} is the number of bacterial colonies on Ti control, and C_i is the number of bacterial colonies on Ti-Ag/Ca, Ti-Ca, or Ti-Ca.

ROS Levels in Bacteria: The 2',7'-dichlorofluorescin-diacetate (DCFH-DA)/ 4'-6-diamidino-2-phenylindole (DAPI) counter-staining assay was applied to determine the burst of intracellular reactive oxygen species (ROS) levels in the bacterial cells cultured on the samples for various durations. The oxidation of non-fluorescent DCFH-DA to fluorescent 2',7'-dichlorofluorescein (DCF) provides a procedure for detection of ROS formation.[3] The bacterial seeding procedure was the same as that described in *Cell Morphology Evaluation*. The samples, after being incubated at 37 ^{o}C for 1, 3, and 5h,were rinsed once with physiological saline, stained with 10 mM DCFH-DA (at room temperature for 30 min), rinsed twice by saline, fixed with 4% paraformaldehyde (PFA, at room temperature for 10 min), and counter-stained using 4'-6-diamidino-2-phenylindole (DAPI, 1μg /ml, at room temperature for 5 min). Afterwards, the samples were observed immediately on a fluorescence microscopy (Olympus GX71).

1.3 Assays for Assessing the Responses of Mammalian Cells

Spreading of BMSCs: The rat bone marrow stem cells (BMSCs, bought from Shanghai Institutes of Biological Science, Shanghai, China) were seeded on the samples (10 mm square plates) at a density of 5.0E4 cells/ml (1 ml/well). An hour or

24h later, the cells were washed with the phosphate buffer saline (PBS), fixed with 4% paraformaldehyde solution (Sigma) for 20 min at room temperature, and permeabilized with 0.1% (v/v) Triton X-100 (Amresco) for 2 min. Then, the cells were stained with FITC-Phalloidin (Sigma) and DAPI (Sigma) at room temperature in the dark. The F-actin and nuclei of the cells were examined on a fluorescence microscopy (Olympus GX71).

ALP and OCN activity in BMSCs: After culturing with cells for 1, 3, 7 days, the specimens were rinsed three times with PBS, and the total RNA of the cultured cells was extracted by a TRIZOL reagent (Invitrogen). One milligram of RNA from each specimen was reverse transcribed into cDNA by a PrimeScript RT reagent kit (TaKaRa) according to the manufacturer's protocols. Real-time polymerase chain reaction (RT-PCR) was performed on a Bio-Rad iQ5 real time PCR system using amixture of SYBR Premix Ex Taq II (TaKaRa), cDNA templates, and the primers. The alkaline phosphatase (ALP) and osteocalcin (OCN) levels in BMSCs were analyzed with glyceraldehyde-3-phosphate dehydrogenase (GAPDH) serving as an endogenous house-keeping gene for normalization. The primer sequences of the genes were shown in **Table S1**. Quantification of the gene expressions was based on the comparative cycle-threshold method.

1.4 Statistical Analysis

Statistical comparisons were carried out via one-way ANOVA and SNK post hoc based on the normal distribution and equal variance assumption test. All statistical analysis was carried out using SAS 8.2 statistical software package.

2 Electrochemistry of Internal Galvanics

Dissimilar phase constitutions have different electrode potentials, and when they come into contact in an electrolyte, one constitution acts as anode and the other as cathode, and such an electrochemical process was termed as 'internal galvanic corrosion' (and the couples of the phases involved in these reactions termed as 'galvanics' in this study).[4, 5] The corrosion rate of the galvanics is theoretically determined by its galvanic current, I_g, which can be expressed as [6-8]

$$I_g = E_\Delta / (R_a + R_c + R_s + R_m), \quad (1)$$

where R_a, R_c, R_s, and R_m are the resistances of the anode, cathode, electrolyte path (from the anodic area to the cathodic area), and the support path (or contact interfaces between the anode and cathode), respectively. E_Δ, electropotential difference between the cathode and anode, is the driving force for an accelerated attack on the anode constitution, which dissolves into the electrolyte. As a result, cathodic proton consumption and anodic metal ion production reactions can be established. As to the Ag/Ca galvanics on the Ti-Ag/Ca group, the silver nanoparticles (Ag NPs) act as the cathode, calcium serves as anode, and the Ti matrix plays as the support path. Accordingly, the anodic reaction occurs via equation (2) to produce calcium ions near the titanium surface:[9-11]

$$\mathrm{Ca} \rightarrow \mathrm{Ca}^{2+} + 2e^-, \quad (2)$$

Calcium ions (Ca^{2+}) release into the surrounding solution (cell culture medium) and electrons (ne^-) are transported from the titanium matrix to the Ag NPs where these

electrons are consumed by the cathodic reactions by equations 3, 4, 5, and 6, which depend on the availability of oxygen and the pH of the solution:[12-15]

$$2H^+ + 2e^- \rightarrow H_2 (pH < 7.0), \quad (3)$$

$$2H_2O + 2e^- \rightarrow H_2 + 2OH^- (pH \geq 7.0), \quad (4)$$

$$O_2 + 4H^+ + 4e^- \rightarrow 2H_2O (pH < 7.0), \quad (5)$$

$$O_2 + 2H_2O + 4e^- \rightarrow 4OH^- (pH \geq 7.0), \quad (6)$$

In the acidic solution, reactions 3 and 5 are prevalent on the cathode, while in a neutral or basic solution that is reactions 4 and 7. It is obvious that equations 3 and 5 are proton consuming reactions, which may occur when acidic extracellular species are involved in cell adhesion.[16] Equations 4 and 6 are also proton consuming reactions because the diffusion coefficient of H^+ is 9.311E-5 cm^2s^{-1} which is about twice that of OH^- (5.273E-5 cm^2s^{-1}),[17] and the OH^- produced from reactions 4 and 6 can further react with protons to form water adjacent to the silver cathodes. That is all the cathodic reactions (equations 3, 4, 5, and 6) consume protons.

Accordingly, the bubbles observed on the Ti-Ca and Ti-Ag/Ca groups (**Figures 2B and D; Figure S4**) are probably produced by the cathodic reactions subjected to this internal galvanic mechanism. In addition, the concentration of calcium liberated in the first day by Ti-Ca and Ti-Ag/Ca was about 750nM and 580nM per square centimeter respectively (it maintained such levels for at least 28 days, the longest time point we have checked). The concentration of calcium released by Ti-Ag/Ca was over three quarters of that released by Ti-Ca; however, the integrated calcium concentration (calculated according to the XPS depth profiles of silver and calcium on corresponding samples, **Figure S3**) in Ti-Ag/Ca was only approximately a quarter of

that in Ti-Ca. Taken together, it can be concluded that silver can help the release of calcium.

3 Breaking the ROS Homeostasis in Bacteria

ROS Generation and Homeostasis in Bacteria: The bacterial cytoplasmic membrane, served as the respiratory center, contains integrated protein complexes (complex I, II, III, IV, etc., which are referred as *Proton pump* in **Figure 2** in the manuscript) that establish a complicated electron transport chain (ETC).[18] As shown in **Figure S8**, tricarboxylic acid (TCA) cycle produced nicotinamide adenine dinucleotide hydrate (NADH) transfer hydrogens (a hydrogen consists of a proton and electron) to ETC, which suttles electrons from complex I to complex IV and to a terminal electron acceptor such as oxygen. The electrons are sequentially caried along the ETC while the protons are suttled to the outside of the membrane. Some of the electron carriers in the ETC, such as complexes III and IV, accept protons from the inside of the bacterial membrane as they accept electrons. The protons are then traported through the membrane as electrons move down the chain. This increases the transmembrane proton gradien and produces a proton motive force (PMF) that drives the synthesis of adenosine triphosphate (ATP) by ATP synthase (ATPase).[19,20] In addition, during bacterial respiration (ETC), a small amount of the oxygen is not reduced completely, resulting in the formation of oxidative byproducts, the reactive oxygen species (ROS) such as superoxide radical ($O_2^{\bullet -}$), hydrogen peroxide (H_2O_2), hydroxyl radical (OH•).[21-23] Appropriate level of ROS plays beneficial physiological roles in various cellular signaling systems,[24] whereas breaking the ROS homeostasis does harm to the maintenance and growth of bacterial cells.[25] Accordingly, the bacterial cells regulate the ROS level by syntehsis of various antioxidant enzymes

(such as superoxide dismutase, catalase, and peroxidase) and catalyzing those reactive species into ordinary molecular oxygen (O_2) or water (H_2O).[26-28]

Effects of Ag/Ca Galvanics on Breaking the ROS Homeostasis: The Ag/Ca galvanics have two synergistic actions to bacterial cells, i.e. cathodic proton consumption and anodic calcium production. The former action depresses the PMF-dependent activity of ATPase and the synthesis of ATP, which further impacts on the ATP-dependent functions in bacteria, such as the efflux of calcium, the synthesis of antioxidant enzymes, and the function of ETC. The latter action of Ag/Ca galvanics supplies calcium to bacteria. The relative high intracellular calcium can stimulate the TCA cycle that enhances electron flow into the ETC and makes the whole bacterial cells work faster and consume more O_2, possibly resulting in more electron leakage in ETC and enhancing ROS generation dut to a faster metabolism.[29] Accordingly, the synergistic actions of Ag/Ca galvanics break the ROS homeostasis in bacteria by stimulating ROS generation via calcium release, and depressing antioxidant system via disruption of PMF. The antibacterial assayes (**Figure 2**) have proved the superiority of the Ti-Ag/Ca group (with a reduction rate of 97%) over the Ti-Ag and Ti-Ca groups (there's only one of the two actions, with a reduction rates of 78% and 44%, respectively).

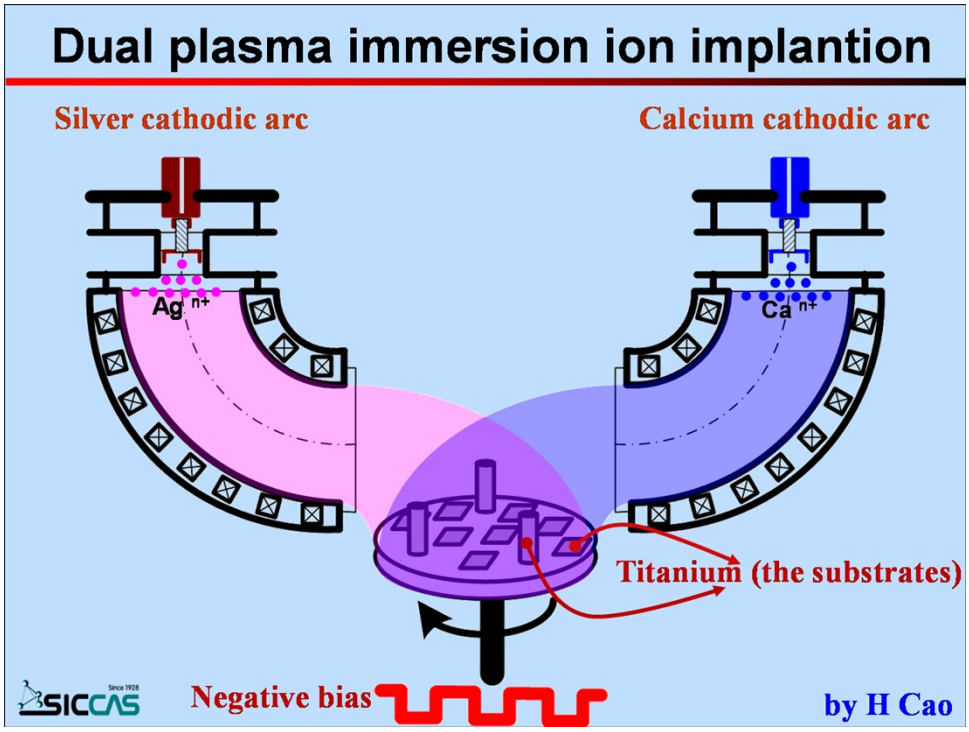

Scheme S1 The plasma immersion ion implantion equipment was set up with two cathodic-arc sources (Dual-PIII process), which synchronously produces positively charged atoms of the corresponding metals, and accelerates the energetic atoms bombarding into the negatively biased titanium substrates.

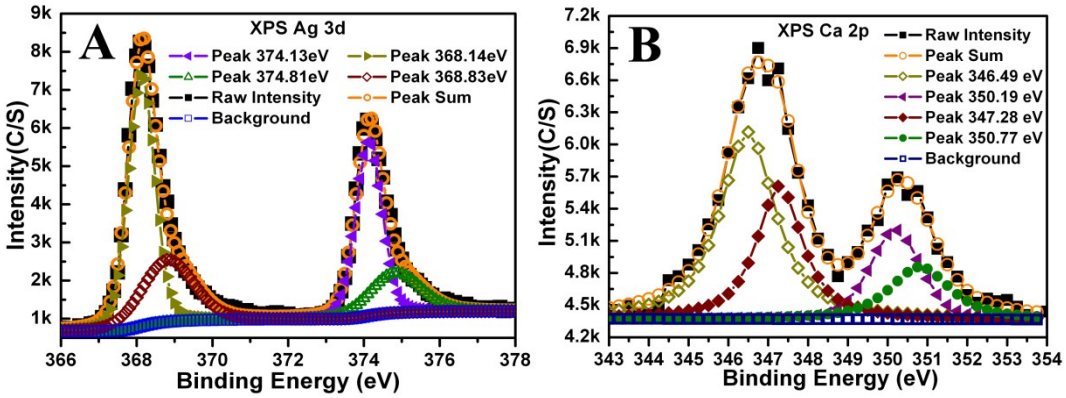

Figure S1 Ag 3d (A) and Ca 2p (B) XPS spectra acquired from the surface of the Ti-Ag/Ca group: the Ag 3d doublets at 368.14 eV /374.13 eV and 368.83 eV /374.81 eV can be assigned to metallic silver and silver alloyed titanium phases respectively;[30] and the Ca 2p doublets at 346.49 eV /350.19 eV and 347.28 eV /350.77 eV correspond to metallic calcium and calcium oxide respectively.[30] The results demonstrated that metallic silver and calcium have been injected onto the titanium substrate successfully.

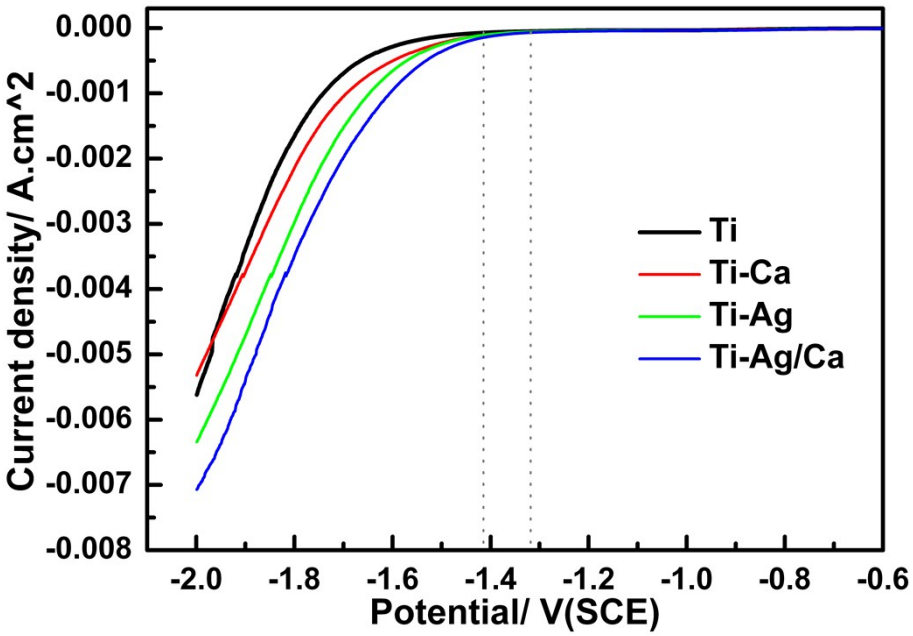

Figure S2 linear sweep voltammetry (LSV) curves: As shown in the Figure, the Ti-Ag/Ca group starts at the potential less negative than that of the Ti-Ag, Ti-Ca, and Ti control, demonstrating that the potential of the hydrogen evolution reaction (HER) on Ti-Ag/Ca group is higher than that on the Ti-Ag, Ti-Ca, and Ti control. This result indicates that the Ti-Ag/Ca group has a stronger potential on influence the proton gradient, which is important to many cell activities.

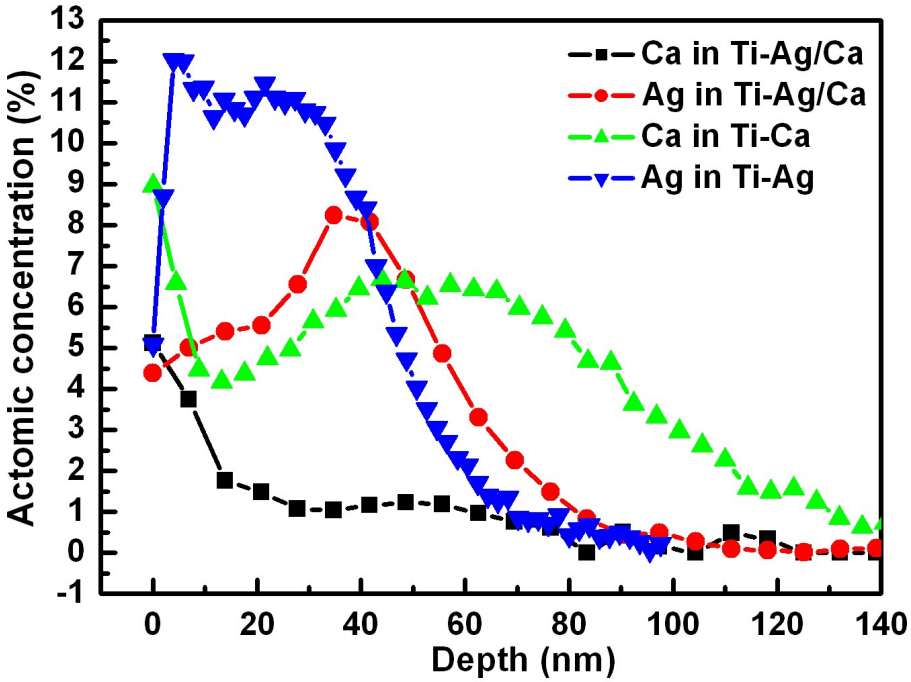

Figure S3 Depth profiles of silver (Ag) and calcium (Ca) on corresponding samples. According to these results, the ratios of the total amount of silver and calcium among the samples can be estimated by integrating the areas made up by the corresponding profile and the horizontal axis. As a result, the integrated calcium concentration in Ti-Ag/Ca was only approximately a quarter of that in Ti-Ca; however, the concentration of calcium released by Ti-Ag/Ca was over three quarters of that released by Ti-Ca (the concentration of calcium liberated in the first day by Ti-Ca and Ti-Ag/Ca, determined by inductively-coupled plasma optical emission spectrometry, was about 750nM and 580nM per square centimeter respectively, and it maintained such levels for at least 28 days), indicating that a galvanic effect was likely established on the titanium surface. This effect has an accelerating effect on degradation of calcium (consequently the amount of calcium released by Ti-Ag/Ca was increased).

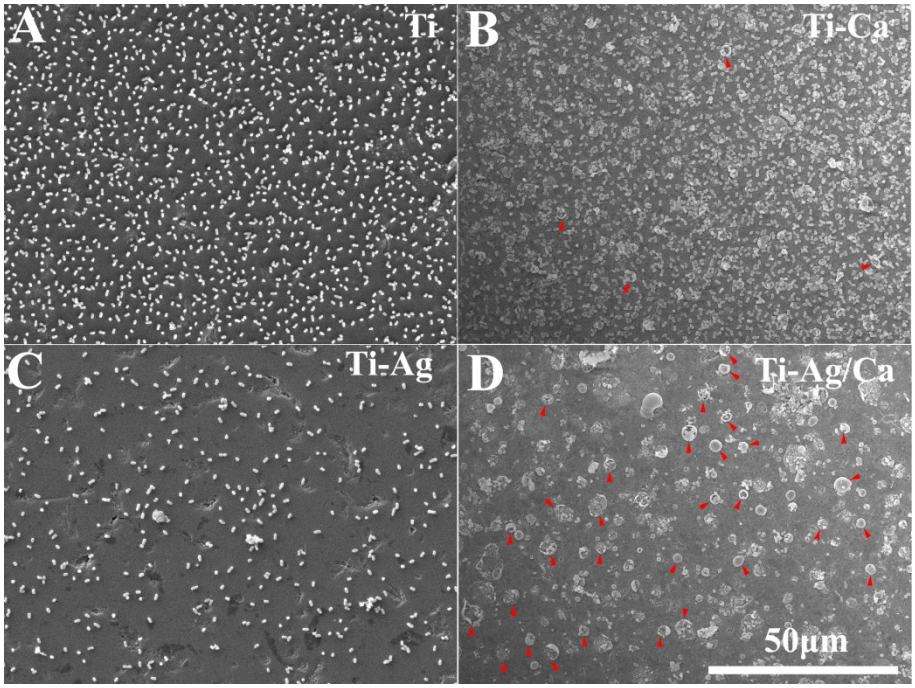

Figure S4 Typical low magnification SEM images of the bacterial cells cultured on the samples for 24h. As shown by the arrows (B and D), micro bubbles were found on both the Ti-Ca and Ti-Ag/Ca groups, but the number of bubbles on the Ti-Ag/Ca group was larger than that on the Ti-Ca group, indicating that the galvanic effect on the Ti-Ag/Ca group was stronger than that on the Ti-Ca group. This was consistent with the accelerating effect on degradation of calcium on the Ti-Ag/Ca groups (detailed in the caption of **Figure S2**).

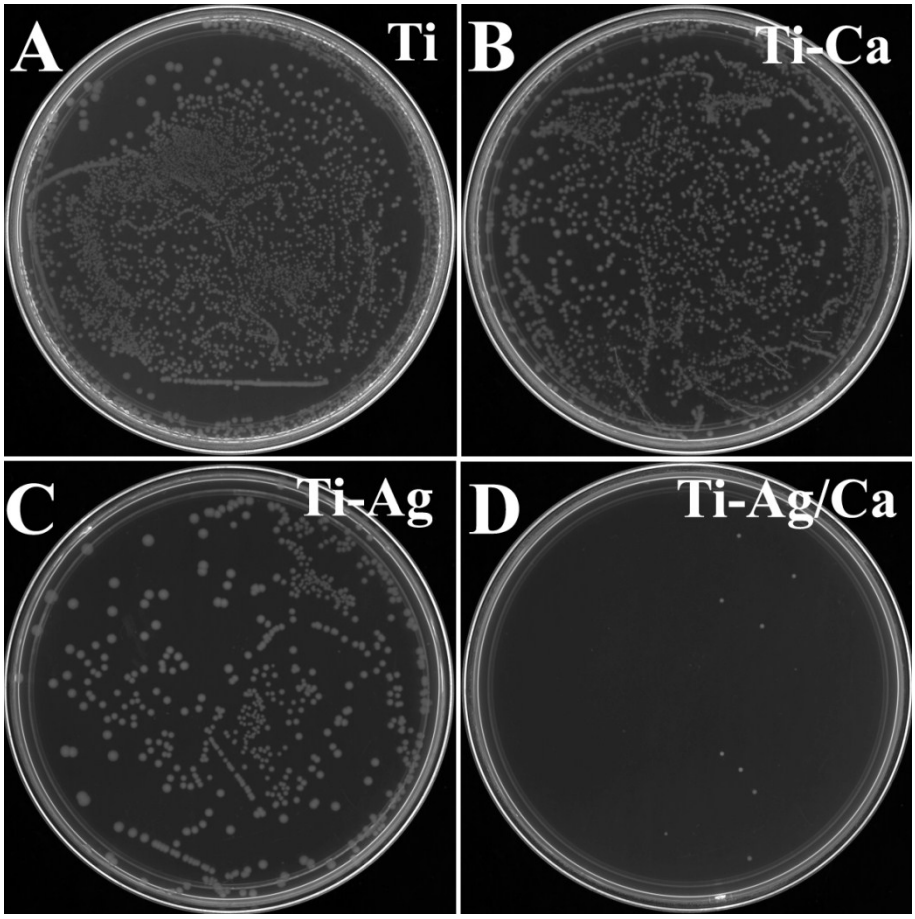

Figure S5 Typical photos of the re-cultivated E. coli colonies on agar: the bacterial cells were previous cultured on the corresponding groups (SEM images of the microbes were shown in **Figure S4**), dissociated by vibration, and then re-cultivated at a dilution of 100 times. The count of these bacterial colonies was shown in **Figure 2E**, and the reduction rate can be calculated according to these results.

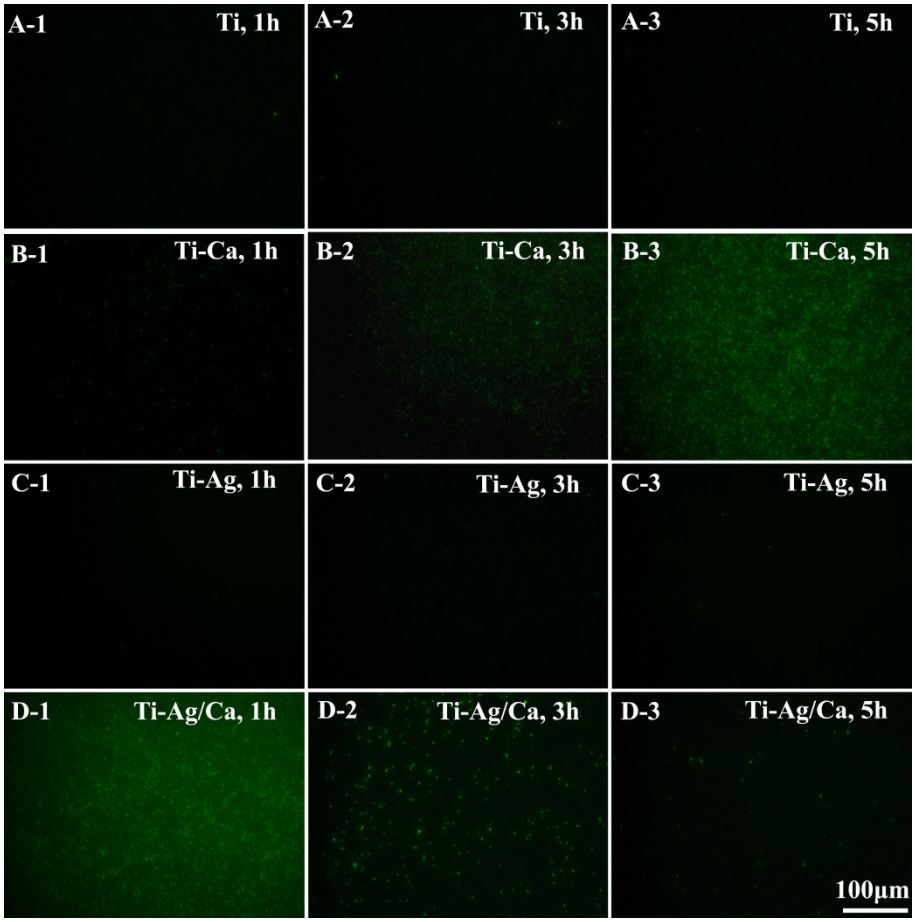

Figure S6 ROS levels in the microbes cultured on the samples for 1(i-1), 3(i-2), and 5h (i-3), i = A, B, C, and D correspond to Ti, Ti-Ca, Ti-Ag, and Ti-Ag/Ca groups. The bacteria were counter-stained with DCFH-DA (transferred to DCF of **green** fluorescence, demonstrating the ROS levels in microbes) and DAPI (**blue**, indicating the total amount of adherent bacteria, shown in **Figure S7**).

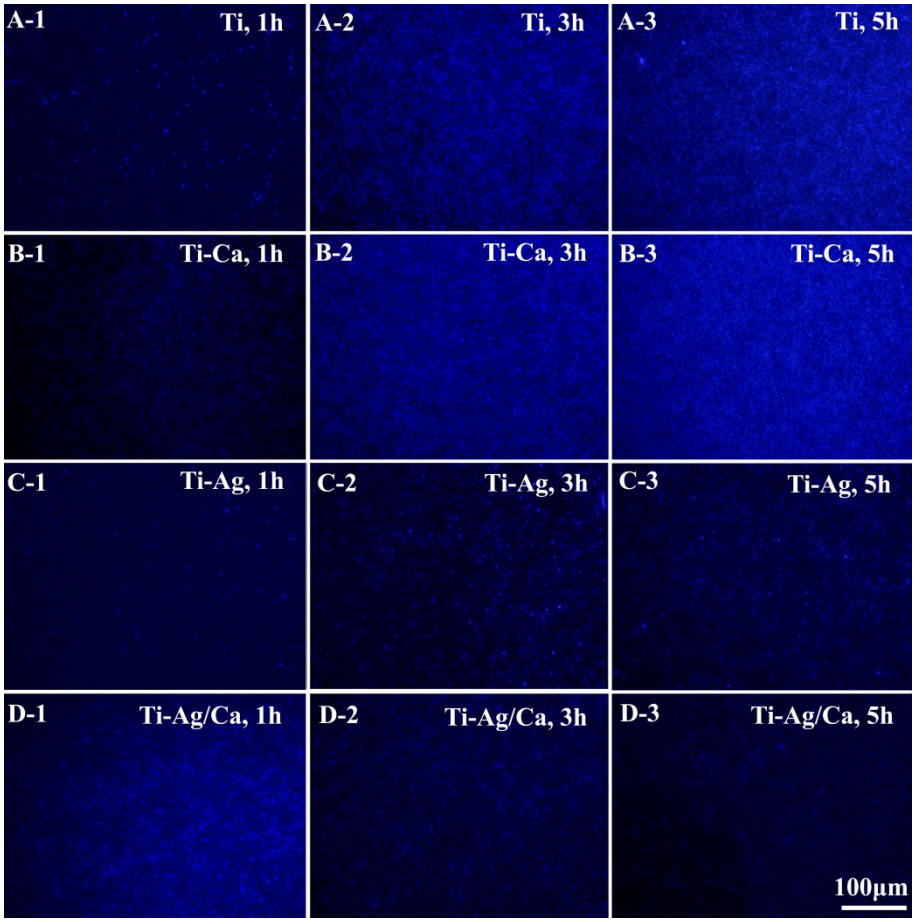

Figure S7 The adherent bacteria on the samples for 1(i-1), 3(i-2), and 5h (i-3), i = A, B, C, and D correspond to Ti, Ti-Ca, Ti-Ag, and Ti-Ag/Ca groups. The bacteria were counter-stained with DCFH-DA (transferred to DCF of **green** fluorescence, revealing the ROS levels in microbes, shown in **Figure S6**) and DAPI (**blue**, indicating the total amount of adherent bacteria).

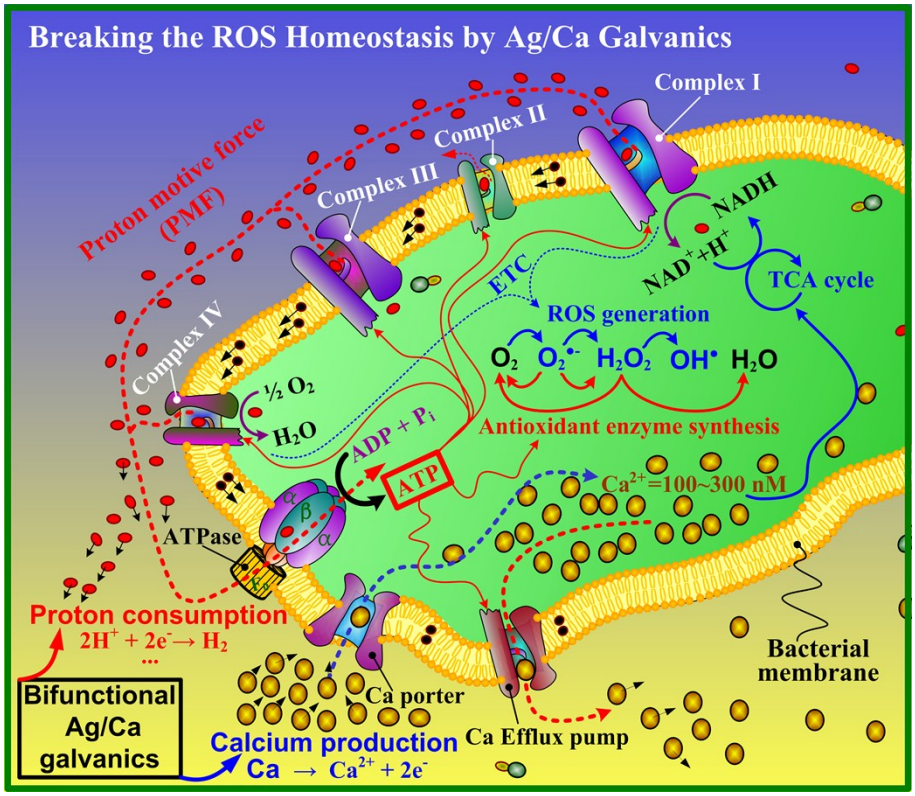

Figure S8. Schematic illustration of breaking the ROS homeostasis in bacteria by the synergistic actions of Ag/Ca galvanics. The Ag/Ca galvanics have two synergistic actions to bacterial cells, i.e. cathodic proton consumption and anodic calcium production. The former action depresses the PMF-dependent activity of ATPase and the synthesis of ATP, which further impacts on the antioxidant system; the latter action of Ag/Ca galvanics supplies calcium to bacteria, which makes the whole cells work faster and enhances ROS generation due to more electron leakage.

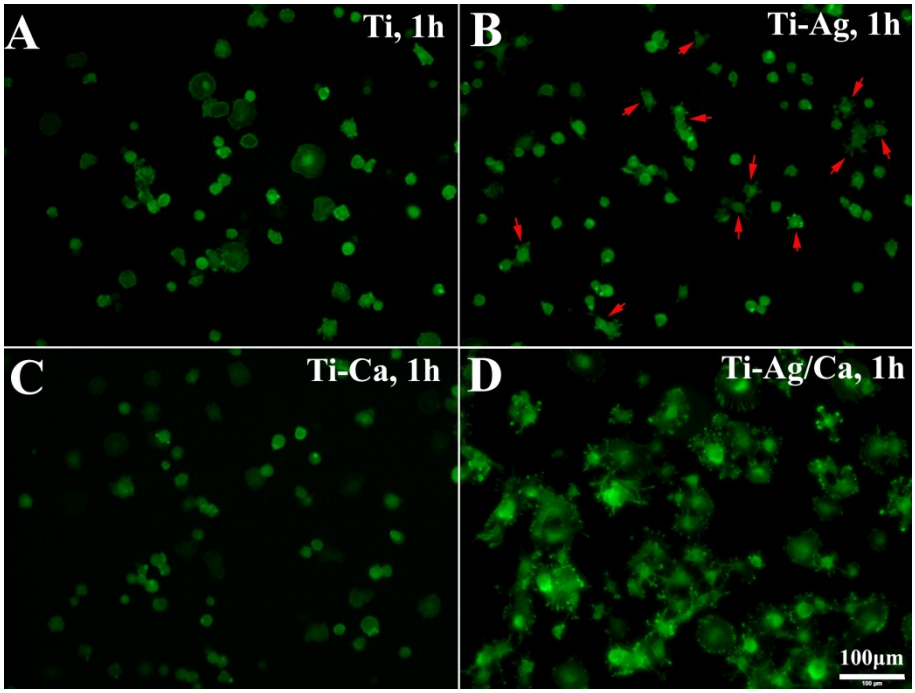

Figure S9 the cytoskeleton (stained with FITC-Phalloidin, **green**, showing the F-actin) of the bone marrow stem cells (BMSCs) cultured on Ti (A), Ti-Ag (B), Ti-Ca(C), and Ti-Ag/Ca (D) for 1h. The area of the spreading cells and the whole SEM images was measured respectively by using Image J. Then the ratio of the two areas were calculated, and this ratio for the Ti, Ti-Ag, Ti-Ca, and Ti-Ag/Ca groups is respectively 9.7%, 9.1%,11.4%, and 36.6%.

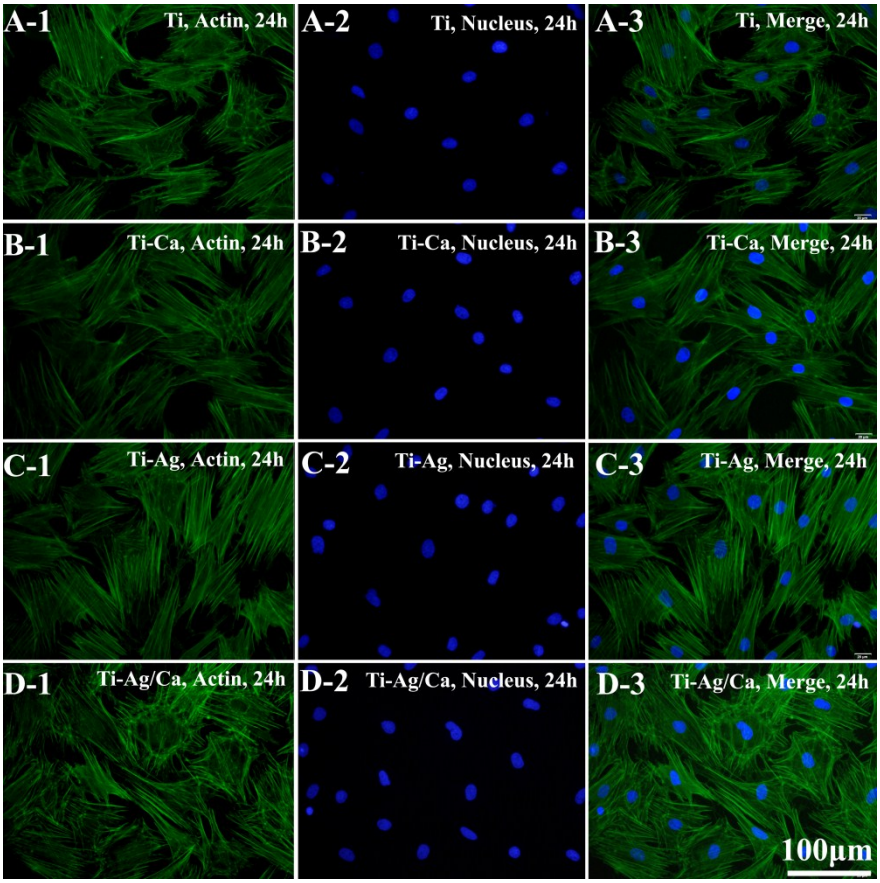

Figure S10 The counter-stained bone marrow stem cells (BMSCs) cultured on Ti (A-i), Ti-Ag (B-i), Ti-Ca(C-i), and Ti-Ag/Ca (D-i) for 24h, i=1 demonstrates the cytoskeleton (F-actin) stained with FITC-Phalloidin (**green**), i=2 shows the nuclei stained with DAPI (**blue**), i=3 is the corresponding merge image of the former two.

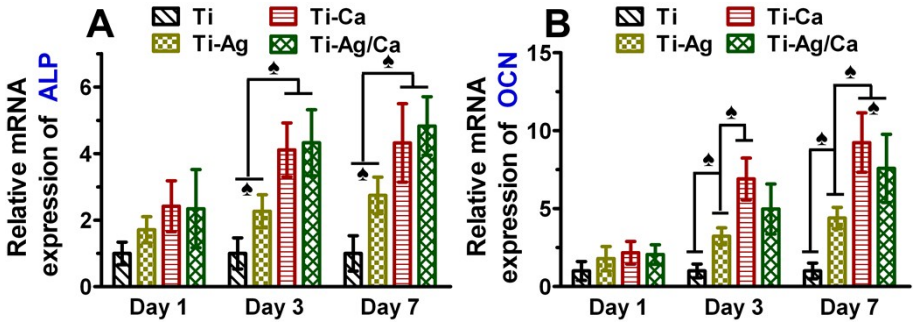

Figure S11 The Ti-Ag/Ca group not only has good antibacterial activity, but also is capable of up-regulating the expression of the alkaline phosphatase (ALP, A) and osteocalcin (OCN, B) levels in BMSCs, which was determined by the real time polymerase chain reaction (RT-PCR) assay, with glyceraldehyde-3-phosphate dehydrogenase (GAPDH) serving as an endogenous house-keeping gene for normalization. The primer sequences of the genes were shown in **Table S1**. Quantification of the gene expressions was based on the comparative cycle-threshold method. ♠, represents $p < 0.05$.

Table S1 Primers for real-time polymerase chain reaction (RT-PCR)

Gene	Prime sequence (F, forward; R, reverse)	Product Size (bp)	Accession number
ALP	F: GTCCCACAAGAGCCCACAAT R:CAACGGCAGAGCCAGGAAT	172	NM_013059.1
OCN	F: CAGTAAGGTGGTGAATAGACTCCG R: GGTGCCATAGATGCGCTTG	172	NM_013414.1
GAPDH	F: GGCAAGTTCAACGGCACAGT R: GCCAGTAGACTCCACGACAT	76	NM_017008.3

Supporting References

1 H. Cao, X. Liu, F. Meng and P.K.Chu, *Biomaterials*, **2011**, 32, 693-705.

2 H. Cao, Y. Qiao, X. Liu, T. Lu, T. Cui, F. Meng and P.K. Chu, *Acta Biomater.,* **2013**, 9, 5100-5110.

3 L. Bourré, S.Thibaut, A. Briffaud, N. Rousset, S. Eléouet, Y. Lajat and T. Patrice, *J. Photochem. Photobiol. B*, **2002**, 67, 23-31.

4 G. Song and A. Atrens, *Adv. Eng. Mater*., **1999**,1, 11-33.

5 K.B. Deshpande, *Electrochimica Acta*, **2011**, 56, 1737-1745.

6 L.J. Liu and M. Schlesinger, *Corros. Sci.*, **2009**, 51, 1733-1737.

7 G. Song, B. Johannesson, S. Hapugoda and D. StJohn, *Corros. Sci.* **2004**, 46,955-977.

8 J. Warkus, M. Raupach and J. Gulikers, *Mater. Corros.,* **2006**, 57,614-617.

9 V.S. Ramachandran, P.J. Sereda and R.F. Feldman, *Nature*, **1964**, 201, 288-289.

10 M.E. Vianna, D.M. Zilio, C.C. Ferraz, A.A. Zaia, F.J. de Souza-Filho and B.P. Gomes, *Braz. Dent. J.*, **2009**, 20, 382-388.

11 D.S. Gibbs and H.J.Svec, *J. Am. Chem. Soc.*, **1953**, 75, 6052–6054.

12 C.Carraro, R. Maboudian and L. Magagnin, Surf. *Sci. Rep.*, **2007**, 62, 499-525.

13 S. Qian, J. Zhang and D. Qu, *Cement Concrete Comp.,* **2006**, 28, 685-695.

14 H. Arslan, H. Celikkan, N. Ornek, O. Ozan, A.E. Ersoy and M.L. Aksu, *J. Appl. Electrochem.*, **2008**, 38, 853-859.

15 J. Warkus, M. Raupach and J. Gulikers, *Mater. Corros.,* **2006**, 57, 614-617.

16 B. Vu, M. Chen, R.J. Crawford and E.P. Ivanova, *Molecules*, **2009**, 14, 2535-2554.

17 O. Guseva, P. Schmutz, T. Suter and O. Trzebiatowski, *Electrochim. Acta*, **2009**, 54, 4514-4524.

18 Y. Anraku, *Annu. Rev. Biochem.*,**1988**,57,101-32.

19 P.D. Boyer, *Annu. Rev. Biochem.*, **1997**, 66, 717-749.

20 N. Nelson, A. Sacher and H. Nelson, *Nat. Rev. Mol. Cell Biol.*, **2002**, 3, 876-881.

21 B. González-Flecha and B. Demple, *J. Biol. Chem.*,**1995**, 270,13681-13687.

22 A.R. Crofts, *Annu. Rev. Physiol.*, **2004**, 66, 689-733.

23 J.A. Imlay and I. Fridovich, *Free. Radic. Res. Commun.*,**1991**,12-13 Pt 1,59-66.

24 B. D'Autréaux and M.B. Toledano, *Nat. Rev. Mol. Cell Biol.*, **2007**, 8,813-824.

25 M.A. Kohanski, D.J. Dwyer, B. Hayete, C.A. Lawrence and J.J. Collins, *Cell*, **2007**,130, 797-810.

26 B.P. Yu, *Physiol.Rev.*,1994, 74,139-162.

27 G. Storz, L.A.Tartaglia, S.B. Farr and B.N. Ames, *Trends. Genet.*,**1990**, 6, 363-368.

28 I. Fridovich, *Science*, **1978**, 201,875-880.

29 P.S. Brookes, Y.Yoon, J.L. Robotham, M.W. Anders and S.S.Sheu, *Am. J. Physiol. Cell Physiol.* **2004**, 287, C817-33.

30 J.F. Moulder, W.F. Stickle, P.E. Sobol and K.D. Bomben, Handbook of X-ray photoelectron spectroscopy. Eden Prairie, MN, USA: Perkin-Elmer Corporation, Physical Electronics Division, **1992**.